Thin Solid Films 612 (2016) 303–309

Contents lists available at ScienceDirect

Thin Solid Films

journal homepage: www.elsevier.com/locate/tsf

On the electrical properties of distinct Eu^{3+} emission centers in the heterojunction GaAs/SnO_2

Cristina de Freitas Bueno, Luis Vicente de Andrade Scalvi *

UNESP - São Paulo State University, Dept. Physics – FC and POSMAT, Post-graduate program in Materials Science and Technology, Bauru, SP, Brazil

ARTICLE INFO

Article history:
Received 17 June 2015
Received in revised form 7 May 2016
Accepted 4 June 2016
Available online 6 June 2016

Keywords:
Tin dioxide
Gallium arsenide
Heterojunction
Electrical properties
Photoluminescence

ABSTRACT

GaAs/SnO_2:2%Eu heterojunctions are deposited by resistive evaporation and sol-gel-dip-coating techniques respectively, with the top layer thermally annealed at different temperatures. The sample annealed at 200 °C/1 h has a much higher conductivity and a lower deepest level (79 meV) than the sample annealed at 400 °C/20 min, for which the deepest level value is 98 meV. The decay of photo-induced current at room temperature for these heterojunctions shows a decay of 48.8% from the initial value for a sample annealed at 200 °C/1 h, compared to a decay of 54.2% from the initial value for a sample treated at 400 °C/20 min. The excitation source has a broad band with energy lower than 1.65 eV, assuring that no electron-hole pair is generated in the SnO_2 (top) layer. The data fitting seems to indicate that, although the grain boundary scattering dominates the mobility, the inclusion of time dependent terms is needed, such as multi-center capture or ionized impurity scattering. Photoluminescence data shows that the main Eu^{3+} transition changes from $^5D_0 \rightarrow {}^7F_2$ (related to ions located at asymmetric sites such as boundary layer) to $^5D_0 \rightarrow {}^7F_1$ (related to ions located at symmetric sites), as the annealing temperature is increased.

1. Introduction

Oxide semiconductor thin films have been matter of growing interest due to its applicability in electronic as well as optoelectronic devices. Luminescent semiconductor thin films can be used in optical communication systems via optical fibers or other sort of systems where photoluminescence or electroluminescence is required. Rare-earth doped wide bandgap semiconductors present luminescent emission with high quantum efficiency [1]. Tin dioxide (SnO_2) is a wide bandgap oxide semiconductor (energy about 3.6 to 4.0 eV) with above 90% transparency in the visible range [2]. Photoluminescence (PL) properties of Eu-doped SnO_2 have been investigated under different lasers excitation [3], and two main locations of Eu^{3+} ions were identified: at symmetric sites, substitutional to Sn^{4+} in the lattice, and at asymmetric sites: the particles surface. In the latter case the location is related to the segregation caused by excess of doping. This behavior may be also related to the particles size, which decreases by increasing the Eu concentration, leading the Eu^{3+} ions to occupy preferentially the surface particle sites. The high intensity close to room temperature is good for technological applications, for instance as electroluminescence devices operating at room temperature. The Eu^{3+} luminescence can be used as an important tool for probing the size of nanoparticles. A variation on the luminescence spectra has been observed when particles grow, because the intensity of the transition $^5D_0 \rightarrow {}^7F_2$ decreases compared to transition $^5D_0 \rightarrow {}^7F_1$. The first is attributed to Eu^{3+} located at surface sites, whereas the second transition is attributed to Eu^{3+} located at lattice sites. A linear relationship between asymmetry and particle area-volume ratio was observed, and correlated with the number of distorted Eu^{3+} surface sites. [4].

Concerning the electrical properties, incorporation of Eu^{3+} in the SnO_2 layer leads to high charge compensation since the rare-earth doping acts as acceptors in the n-type matrix. Besides, it decreases the crystallite size, increasing the grain boundary electronic scattering [5]. Surprisingly, results of electrical conductivity for Eu^{3+}-doped SnO_2 nanocrystals, indicate higher conductivity for doped samples [6]. On the other hand, gallium arsenide (GaAs), used in this paper as the bottom layer for the heterojunction GaAs/SnO_2:2 at%Eu^{3+}, is a high mobility semiconductor with zinc blend tetragonal structure. In the single-crystal form its bandgap is about 1.42 eV.

Heterojunctions may be an interesting way of improving the properties of the individual films. Heterojunctions using transparent oxides deposited on top of semiconductors have been presented recently. High-quality self-textured ZnO films has been grown on top of a GaAs substrate, forming a heterojunction with characteristic of rectifying diode, with blue-violet and infrared electroluminescence [7], suitable for optical fiber telecommunications applications. Promising devices for the development of solid-state lighting were achieved by *n*-ZnO/*n*-GaAs heterostructured light-emitting diodes [8]. Other combinations of semiconductor heterojunctions with SnO_2 have been successfully

* Corresponding author.
E-mail address: scalvi@fc.unesp.br (L.V. de Andrade Scalvi).

http://dx.doi.org/10.1016/j.tsf.2016.06.008
0040-6090/

used such as with gallium selenide (GaSe) [9]. Heterostructures of semiconductors monolayers transition-metal dichalcogenides (TMDC), with interfaces of atomic precision, leads to high quality optical properties, suggestion application in optoelectronic devices, such as photodiodes, photovoltaic cells or photodetectors [10,11]. Controlling the crystalline face in the heterojunction coupling leads to a smart design of assemblies with adequate charge separation and improved photocatalytic performance. The heterojunction junction $BiVO_4$-110-TiO_2 has high capacity of charge-carrier separation and better photocatalytic performance than the combination $BiVO_4$-010-TiO_2 [12]. This fact can be attributed to the better electron fluidity from the plane (110) of $BiVO_4$ to TiO_2, due to lower interface barrier. Combination of perovskite layers with fluor-doped thin oxide (FTO) has allowed building high quality planar heterojunction solar cells [13,14], where it has been proposed a Volmer—Weber growth mechanism [15]. Deposition of heterojunctions with smooth and atomic quality surfaces has become a possibility since the growth of epitaxy layers became available. This sort of deposition may lead to the formation of a quantum well at the interface, due to the interrupting atomic band diagrams of distinct materials. This quantum well may present energy levels below the conduction band bottom of one or both materials and, may give birth to a two-dimensional electron gas (2DEG) [16]. Such structure spatially separates conduction electrons and donor impurity atoms, reducing the influence of ionized and neutral impurity scattering on the electron motion.

The SnO_2 and GaAs combination may improve the electrical properties, as have been reported previously [17,18]. The junction of these two materials leads to a discontinuity in the valence and conduction bands, due to the Fermi level equality condition. The band bending at interface may create the 2DEG, a region with high electron concentration and confinement. The Eu^{3+} emission in SnO_2 can be significantly improved when the oxide layer is grown on top of a GaAs layer [19]. Then, in order to acquire deep knowledge on this sort of devices, the electrical properties must be investigated.

The n-type conduction of SnO_2 is caused mainly by oxygen vacancies, generated during the crystal growth process, which causes insulating metallic oxides to behave as semiconductors. Then, the control of vacancies into these materials leads to transparent coatings with tunable electrical conductivity [20], which turns out to be a very desirable property to be explored for improving device properties, such as in gas sensors and transparent conductive coatings. The phenomenon of persistent photoconductivity (PPC) [21] has been found in rare-earth doped SnO_2 [22]. More recently, PPC has been found in SnO_2 nanobelts [23] and quantum dots [24]. Modeling the decay of PPC, mainly considering the nanosized grains of sol-gel SnO_2 has led to important parameters of the electron transport kinetics, such as energy capture and grain boundary potential barrier [25].

In this paper the current decay of photo-induced conductivity is measured at room temperature and the model to fit the trapping kinetics by ionized centers is revisited. Besides, temperature dependent resistivity is shown, and the variation in the dominant Eu^{3+} emission in the PL spectra is discussed as well. The contribution is the knowledge on electrical properties of a selective emitting assembly, which can be coupled to design electroluminescent devices.

2. Experimental details

2.1. Thin film deposition

GaAs thin films were deposited by the resistive evaporation technique, in a BOC Edwards evaporator system Model AUTO 500. GaAs tiny pieces were placed on a tungsten boat inside a low pressure chamber (10^{-5} mbar), allowing the sublimation by circulation of electrical current through the metallic boat. The rotation of the substrate holder (round plate) assures homogeneous composition and thickness of deposited films. After evaporation, films where submitted to a thermal annealing at 150 °C by 30 min in an EDGCON 3P oven.

The deposition of Eu^{3+}-doped SnO_2 thin film layer was described in details elsewhere [3]. The deposition takes place in air atmosphere (room temperature), and after each layer, samples are dried in air by 20 min and treated at 200 °C by 10 min in the same oven used for GaAs annealing. This procedure was repeated 10 times. The final annealing was at 200 °C by 1 h (sample H1) or 400 °C by 20 min (sample H2). Another sample, a SnO_2:2%Eu thin film, was deposited directly on quartz substrate, and the final annealing was 1000 °C by 1 h (sample FF1). The electrical contacts to the heterojunctions were made from In deposition also by resistive evaporation.

2.2. Electrical characterization

Electrical characterization was carried out using a Keithley electrometer model 6517. Sample was placed in a Janis He-closed cycle cryostat with a compressor CTI-Cryogenics, coupled to a Lake-Shore temperature controller, which controls the temperature with precision of 0.05 K. Measurements include the evaluation of resistance as function of temperature, and the decay of photo-induced conductivity. In the case of this former experiment, a halogen-tungsten lamp was used as excitation source, coupled to a filter, which cutoff wavelength below 750 nm (energies higher than 1.65 eV), assuring that no electron-hole pair is generated in the SnO_2 (top) layer. In other words, only intrabandgap levels of SnO_2 can be excited. The procedure detail of this experiment has been published elsewhere [25] and consists, basically, of measuring the optically generated metastable current as function of time. The time for saturation was assumed as 6 min of continuous irradiation. In this paper only room temperature decays were measured.

2.3. Scanning electron microscopy (SEM)

To accomplish scanning electron microscopy (SEM) experiments, samples were fixed at a sample holder (stub) using conducting silver solution. After paint drying, sample was submitted to metallization with a gold layer. Measurements were carried out at a LS15 model from Carl Zeiss or a Quanta 200 model from FEI.

2.4. Photoluminescence setup

For the photoluminescence (PL) measurements in the UV–Vis range, samples were excited with a modulated 350 nm line of a Kryptonium (Kr^+) laser and the signal was detected by a R955 PMT from Hamamatsu and a SR530 Lock-in Amplifier from Stanford Research System. A single configuration monochromator was used for scanning the PL spectra.

3. Decay of photo-induced conductivity

The photo-induced current decay procedure consists, basically, in taking the sample to a fixed and constant temperature, where the sample is irradiated with monochromatic light, after the temperature reaches steady state. Then, the current is measured until it reaches saturation, when the illumination is removed and the current is recorded. Repeating this procedure for several temperatures leads to the determination of relevant parameters of the charge kinetics, such as capture barrier (E_{cap}) of the dominant level and the grain boundary barrier (ϕ) [25,26], since the magnitude of the decay is temperature dependent and becomes slower as the temperature decreases, as reported previously for Er-doped [25] and Eu-doped SnO_2 [27]. The measurement carried out here has two major modifications when compared to the previous published setup: 1) it was carried out only at room temperature, 2) instead of monochromatic light it was used a halogen-tungsten lamp as excitation source, coupled to a filter, which cutoff

wavelength below 750 nm (energies higher than 1.65 eV), assuring that no electron-hole pair is generated in the SnO_2 (top) layer.

In order to model the current decay, the current as function of time, for a fixed temperature is given by:

$$i(t) = K_S \cdot n(t) \cdot \mu(t) \cdot q \tag{1}$$

where K_S is a constant relating current and conductivity, $n(t)$ is the time dependent electron concentration, $\mu(t)$ is the time dependent electronic mobility and q is the electron charge. X-ray diffraction data for these films (not shown) exhibits a diffuse shape profile, typical of small crystallite domain. The average crystallite size evaluated from line broadening XRD pattern is about 7 to 20 nm as will be seen below, in good agreement with previous publication [28]. Then, electrical transport dominated by grain boundary scattering seems to be an adequate hypothesis, since the grain size is very small. The mobility due to grain boundary scattering is proportional to $T^{-1/2}\cdot\exp(-\phi\cdot k^{-1}T^{-1})$ [29], where ϕ is the grain boundary potential barrier and k is the Boltzmann constant. Then, it depends only on the temperature, since the grain boundary potential barrier shall not change for the current decay in a fixed temperature, and then, $\mu(t)$ must be a constant.

The decay rate of photo-induced electrons from the conduction band is given by:

$$\frac{dn}{dt} = -V_{th}\gamma_n \cdot n \cdot N_{DEF}^{+} \tag{2}$$

Where V_{th} is the electron thermal velocity ($=3$ kT/m*, where m* is the conduction band effective mass), n is the electron concentration in the conduction band and N_{DEF}^{+} is the ionized defects concentration, which can be oxygen vacancies or Eu^{3+} centers, but with distinct capture time intervals. Besides, it is assumed that defects have simple ionization so that $N_{DEF}^{O} \rightarrow e^{-}{}_{+}\, N_{DEF}^{+}$ and $N_{DEF}^{+} = n$. γ_n is the capture cross section, which is given by:

$$\gamma_n = \cdot\gamma_\infty \cdot \exp\left(-\frac{E_{cap}}{kT}\right) \tag{3}$$

where γ_∞ is the cross section constant and E_{cap} is the capture barrier energy. Then, taking into account the solution of simple differential Eq. (2), the current as function of time can be given by:

$$i(t) = K_S \frac{\sigma(0)}{1 + n(0) \cdot C_1 \cdot t} \tag{4}$$

where C_1 is the product of V_{th} and γ_n, $\sigma(0)$ and $n(0)$ are the initial conductivity and initial free electron concentration, respectively.

4. Results and discussion

4.1. Electrical properties

Fig. 1 shows electrical current for an applied bias of 20 V for the heterojunction GaAs/SnO_2:2%Eu thermally annealed at 200 °C/1 h (sample H1) and 400 °C/20 min (sample H2). The superior inset shows the evaluation of the deepest energy level of defect, ionized close to the room temperature, whereas the inferior inset is the evaluation of the resistivity, obtained from the current data and sample dimensions (distance between contacts: 0.5 cm; films thicknesses: GaAs, 282 nm, SnO_2, 300 nm; contact width: 1.0 cm). It is observed that the current for sample H1 is much higher, changing from microampere to nanoampere (sample H2). The slope of the curve in the superior inset changes continuously, suggesting the existence of a defect level distribution, which is rather acceptable for this sort of samples, with random distribution of neighboring atoms, characteristic of materials with nanocrystals as building blocks. However, at least two levels are clearly detected: one at low temperature and the deepest level, ionized

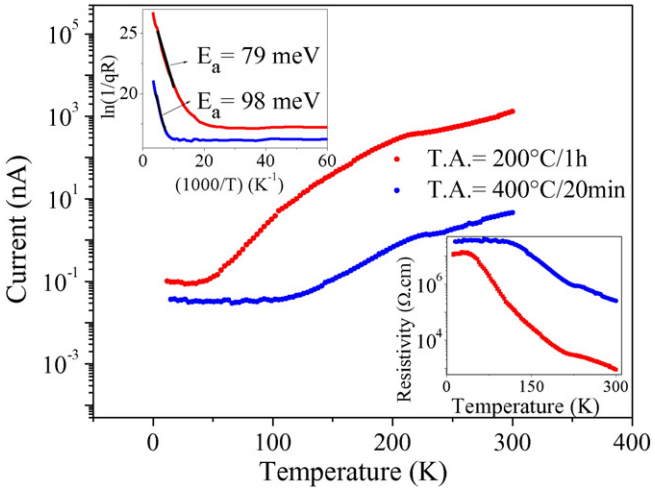

Fig. 1. Current as function of temperature for heterojunctions GaAs/SnO_2:2%Eu with thermal annealing at 200 °C/1 h (H1) and 400 °C/20 min (H2). Upper inset activation energy evaluation for both samples. Lower inset: electrical resistivity.

around room temperature. The activation energy of this deepest level is 79 meV, for sample H1 and 98 meV for sample H2. This difference in the activation energy values may explain the difference in the current magnitude for these two samples. Surprisingly, the sample treated at lower temperature and, then, with smaller crystallites (as will be shown below), presents a shallower energy level, which is more easily ionized, leading to a higher current. Concerning the resistivity curves, at the inferior inset, it is observed that they present similar behavior, even though the sample treated at 200 °C presents lower resistivity and a broader variation for the whole temperature range investigated.

Fig. 2 presents the decay of photo-induced current for both heterojunction samples. The decay for the heterojunction GaAs/SnO_2:2%Eu, thermally annealed at 200 °C/1 h (sample H1), is shown in the main Fig. 1, whereas the decay for the heterojunction treated at 400 °C/20 min (sample H2) is shown in the inset of Fig. 2. The excitation source assures energies lower than 1.65 eV, with no electron-hole pair generated in the SnO_2 (top) layer, and only intrabandgap levels of SnO_2 are excited. However, if the intensity is high enough, the light may penetrate into the GaAs layer and generate electron-hole pairs in this material. Besides, there is possibility of excitation of the 2DEG [17, 30]. Fig. 3 illustrates this situation, showing on the right side the ionization of impurities in the SnO_2 layer (top), which present a distribution of

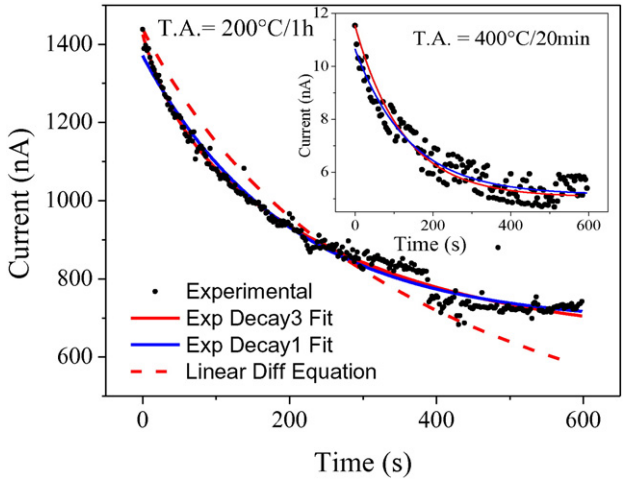

Fig. 2. Decay of photo-induced electrical current for heterojunction sample GaAs/SnO_2:2%Eu treated at 200 °C/1 h and fitting procedures. Inset: same sort of measurement for the heterojunction treated at 400 °C/20 min.

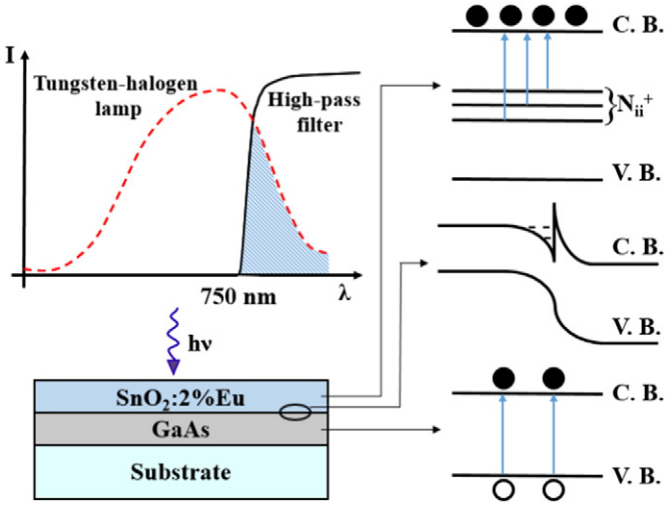

Fig. 3. Schematic diagram of sample layout and photoiunduced carrier generation. At left, top, the spectra of excitation source plus filter, at bottom, the sample layout. At right, top: intrabandgap impurity ionization of SnO_2 layer, center: 2DEG, bottom: electron-hole generation at GaAs layer.

energy levels (due to disordered neighborhood), the possibility of 2DEG formation at GaAs/SnO_2 interface (center), and the electron-hole generation in the GaAs layer (bottom). The electrical current in the excitation lamp was 5.5 A (low intensity) and the excitation time was 6 min. The applied bias on the sample H1 was 20 V. Just after the lamp was turned off, the sample current was 1.4 μA, and after 600 s it decays to 0.74 μA, which means a variation of 48.8% from the initial value. For the sample H2, the same measurement conditions were set for the decay evaluation, and the data is plotted in the inset of Fig. 2. In this case the initial electrical current was 11.4 nA, and after 600 s it decayed to 5.2 nA, which means a variation of 54.2% from the initial value. For this H2 sample, the same sort of measurement, carried out at 250 K, led to a decay of 65.7% of the initial value, which means that although the electron trapping is a thermal influenced phenomena, it presents some peculiarities in these heterostructure samples.

Comparing the decays obtained for both heterostructure samples (annealed at different temperatures), the higher variation (current decay) takes place for the sample H2, annealed for 400 °C/20 min. This sample also presents higher activation energy (98 meV), as shown from Fig. 1, when compared to sample H1 ($E_a = 79$ meV). This is an interesting result, because the deeper defect level acts as a more efficient driving force for retrapping the excited electrons. Concerning the measurement carried out at 250 K for the H2 sample, it is possible to verify that it decays faster than at room temperature, showing the same sort of behavior found by Floriano et al. [26] for Sb-doped SnO_2 thin films, in opposition of what is expected for a thermal induced process, and found in previous papers, when the excitation source has energy above the bandgap energy [25,27]. Another interesting feature is that the electrical current always returns to the original value at room temperature, rather uncommon phenomena on dealing with SnO_2 thin films.

On the other hand, the fitting procedure for the experimental curve hardly follows Eq. (4), as can be seen by the broken red line in Fig. 2. In order to fit the decay data two other fittings are proposed: an exponential decay: blue line and Eq. (5) and a three-exponential decay: red line and Eq. (6). The parameters used in these fitting procedures are summarized in Table 1. The physical meaning of used parameters is related to the upcoming discussion.

$$i = i_0 + A_1 e^{\frac{-(t-t_0)}{t_1}} \tag{5}$$

Table 1
Parameters for exponential decay and three-exponential decay for samples H1 and H2.

	GaAs/SnO_2:2%Eu (200 °C/1 h)		GaAs/SnO_2:2%Eu (400 °C/20 min)	
	ExpDecay1	ExpDecay3	ExpDecay1	ExpDecay3
i_0 (nA)	684	638	5.15	5.06
t_0 (s)	0.3867	7.199	−6.05	0
A_1(nA)	685	304	5.76	2.16
t_1(s)	196.2	266.6	138.6	123.6
A_2(nA)		305		2.16
t_2(s)		266.7		123.6
A_3(nA)		133		2.16
t_3 (s)		39.3		123.6

$$i = i_0 + A_1 e^{\frac{-(t-t_0)}{t_1}} + A_2 e^{\frac{-(t-t_0)}{t_2}} + A_3 e^{\frac{-(t-t_0)}{t_3}} \tag{6}$$

Considering the poor adjust for Eq. (4), where the grain-boundary-scattering-dominated-mobility is time-independent, there are two possibilities: 1) capture for more than one center, which would have dominant capture for distinct time intervals. That would be in good agreement with previous proposal for the decay fit in Er-doped SnO_2 [25] and Eu-doped SnO_2 [27]; 2) at room temperature, other mechanisms besides the grain boundary scattering must be taken into account for the mobility evaluation. In this case, the Brooks Herring equation for ionized impurity scattering has N_{ii}, the ionized impurity concentration, and n, the free carrier concentration in its formulation [31], which would be time-dependent terms. An analysis of the transient decay of persistent conductivity based on ionized impurity scattering has been presented in the past, based on Brooks Herring equation [21] or Takimoto screening correction [32,33]. At room temperature, it seems reasonable to take the lattice scattering into account. However, as the phonon concentration does not vary with time for fixed temperatures, it should have no contribution for this decay, since the temperature is constant.

Actually, we believe that the deviation from the simple linear differential equation solution for the free carrier concentration, and, thus, the current decay come from a combination of these two possibilities: a variation in the concentration of scattering centers as the electron capture takes place during the decay as well as distinct trapping centers at different time intervals (such as Eu^{3+} centers and oxygen vacancies), as concluded in a previous publication for Eu-doped SnO_2 [27]. This interpretation is coherent with the fact that the best fit is a three exponential equation (mainly at the beginning of the data) compared to the single exponential, as can be seen in Fig. 2.

4.2. Scanning electron microscopy

Fig. 4 shows SEM images of the surface for the heterojunction layers: Fig. 4a is the image for the GaAs layer thermally annealed at 150 °C by 30 min, Fig 4b is the surface of the SnO_2:2%Eu thin film annealed at 500 °C by 1 h, Fig 4c is the surface of the heterojunction GaAs/SnO_2:2%Eu, where the top layer is annealed at 400 °C by 20 min, and Fig. 4d shows the surface of heterojunction GaAs/SnO_2:2%Eu, treated at 200 °C by 1 h. It is easily seen in Fig 4a that the GaAs layer presents round shaped particles with a rather uniform size distribution, whereas the SnO_2 film grown directly on the substrate, presents more uniform surface (Fig 4b). In this case, particles are not easily identified on the sample surface. On the other hand, when the Eu-doped SnO_2 film is grown on top of the GaAs layer, larger sized particles show up at the surface. Comparing Fig. 4c and d, it seems that as the annealing temperature gets higher, the number of particles on the surface increases, suggesting some sort of nucleation on the SnO_2 layer, which may be originated from the particles on the GaAs layer surface and increases with annealing temperature of the SnO_2 layer. In the case of the SnO_2

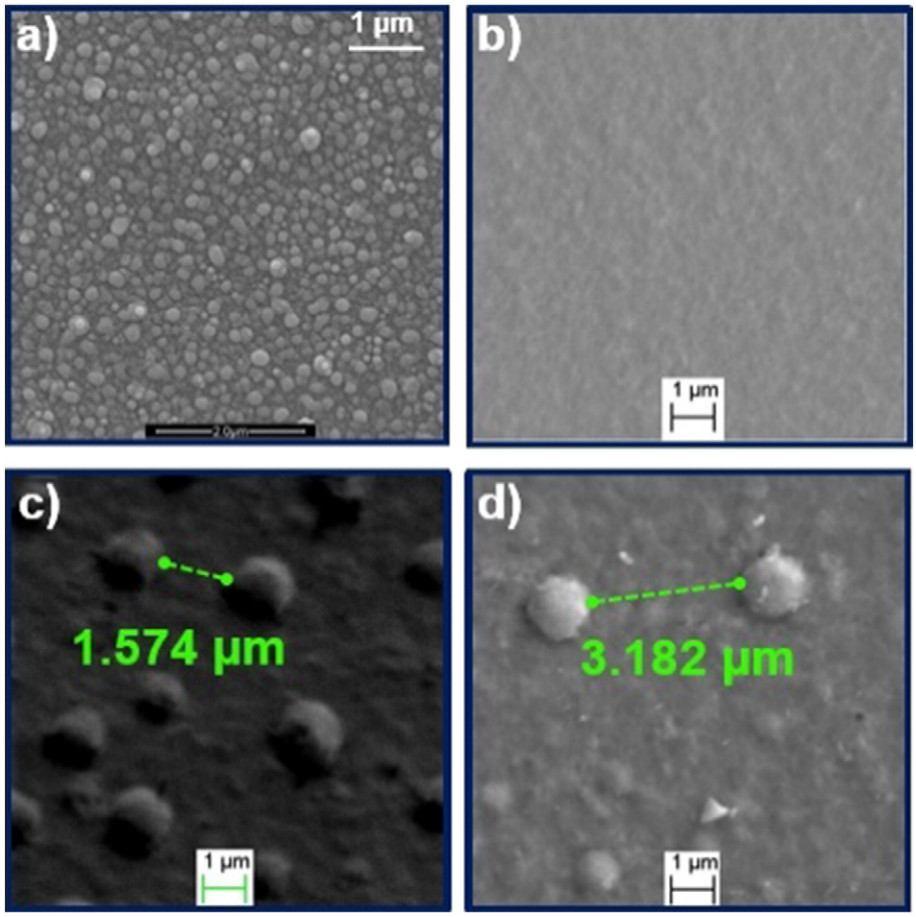

Fig. 4. SEM of the surface: (a) GaAs layer thermally annealed at 150 °C by 30 min, (b) SnO_2:2%Eu thin film annealed at 500 °C for 1 h, (c) heterojunction GaAs/SnO_2:2%Eu, where the top layer is annealed at 400 °C for 20 min, d) heterojunction GaAs/SnO_2:2%Eu, treated at 200 °C by 1 h.

layer treated at 200 °C a typical distance between particles is about 3.2 μm (Fig. 4d) whereas for a sample treated at 400 °C it is about 1.6 μm (Fig. 4c). This observation suggests a Volmer—Weber growth mechanism, a process involving the formation of island shaped grains [15]. Zheng and coworkers [13] have observed that mechanism in the crystallization phenomenon of thermal-induced deposition of dense perovskite layers onto FTO (fluor-doped thin oxide) layer for building of high quality planar heterojunction solar cells [14].

The surface disposition for the heterojuctions shown in Fig. 4c and d may affect the electron scattering for these heterojunction samples and thus, the conductivity. Considering that the sample annealed at lower temperature has fewer visible particles on the surface, it may mean a larger mean free path for the charge carriers for the heterojunction treated at 200 °C. This possibility justifies the higher conductivity for this sample, even though the crystallite evaluated via the Scherrer equation is smaller, as will be seen.

4.3. Emission properties

Fig. 5 shows a part of the photoluminescence spectra (the range 575 nm to 650 nm) of samples of heterojunction GaAs/SnO_2:2%Eu, sample H1 and sample H2, and a SnO_2:2%Eu thin film, sample FF1. The inset of Fig. 5 shows the same spectra, with their intensities normalized by the maximum value in each curve. It is done to improve the visualization of distinct emission bands related do distinct transition processes in each curve. The excitation source is the 350 nm line of a Kr^+ laser. Eu^{3+} transitions $^5D_0 \rightarrow {}^7F_1$ (around 590 nm) and $^5D_0 \rightarrow {}^7F_2$ (about 618 nm) are clearly seen. It is important to recall the nature of the transitions $^5D_0 \rightarrow {}^7F_1$ and $^5D_0 \rightarrow {}^7F_2$, labeled in Fig. 5. The first one is a magnetic dipole transition and its intensity is not affected by structural changes of the nearest neighborhood, whereas the transition $^5D_0 \rightarrow {}^7F_2$ is ruled by electric dipoles, being hypersensitive to the local crystalline field [34]. The asymmetric ratio, defined by the ratio between the lines ($^5D_0 \rightarrow {}^7F_2$)/($^5D_0 \rightarrow {}^7F_1$), indicates dominant emission from excited ion located at symmetric sites for values close to zero, for example Eu^{3+}

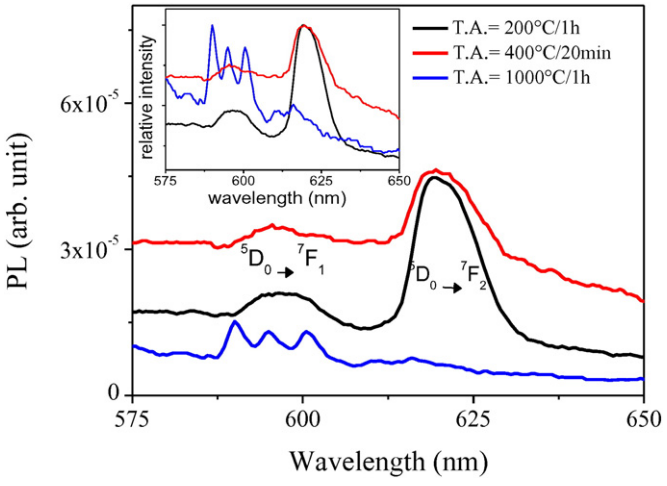

Fig. 5. Photoluminescence of heterojunctions GaAs/SnO_2:2%Eu with thermal annealing at 200 °C/1 h and 400 °C/20 min, and SnO_2:2%Eu thin film deposited on quartz, and annealing at 1000 °C/1 h. Inset: relative intensity, where the same spectra are normalized by the maximum value in each curve, in order to improve the visualization.

Table 2
Crystallite size thin film samples, evaluated by the Scherrer equation.

Sample	$GaAs/SnO_2$:2%Eu (glass substrate) T.A. 200 °C/1 h	$GaAs/SnO_2$:2%Eu (on glass) T.A. 400 °C/20 min	SnO_2:2%Eu 1000 °C/1 h (on quartz)
Crystallite size (101) direction (nm)	7.3	10.9	19.3

substitutional to Sn^{4+} in the SnO_2 lattice [35–37]. On the other hand, an asymmetric ratio higher than 1 indicates dominance of PL from ions located at asymmetric sites such as boundary layer sites. It is clearly seen in Fig. 5 that as the annealing temperature increases the asymmetric ratio decreases, being much higher than 1 for sample H1 (thermal annealing at 200 °C) and close to zero for the sample FF1 (annealing at 1000 °C). Besides, it brings an interesting observation concerning the excitation with the line 350 nm from the Kr^+ laser leads to the $^5D_0 \rightarrow {}^7F_1$ transition as the most intense, unlike excitation with the fourth harmonic of a Nd:YAG laser (266 nm) for the same sort of high doping samples, where the transition $^5D_o \rightarrow {}^7F_2$ turned out as the most intense [3]. 350 nm is close to the value of the SnO_2 bandgap and must be more efficient on the band-to-band excitation and energy transfer to Eu^{3+} substitutional sites.

Table 2 shows the crystallite size, evaluated according to the Scherrer equation in the (101) direction, which corresponds to the most intense peak in the DRX diffractogram (not shown here). The results in table 2 show that as the annealing temperature increases, the crystallite size also becomes larger. Then, the ion located preferentially at crystallite boundary layer, for small crystallites (as the case for the heterojunction thermally treated at 200 °C/1 h), gives place to Eu^{3+} ions located inside the crystallite, substitutional to Sn^{4+}, as the crystallite grows. Then, the $^5D_0 \rightarrow {}^7F_2$ transition gives place to dominance of the $^5D_0 \rightarrow {}^7F_1$ transition. The high annealing temperature also allows splitting the emission lines [38], which becomes more clearly defined.

Another interesting point is that the heterostructure annealed at 200 °C presents smaller crystallites, but a much higher conductivity as seen in Figs. 1 and 2. It is easily inferred that the smaller crystallites implies more ions located at the boundary layer. Then the conductivity increase may be related to a decrease of the potential barrier at grain boundary, since more oxygen vacancies surround the Eu^{3+} impurity doping as concluded for Sb-doped SnO_2 using EXAFS measurements [28]. It also agrees with capture for distinct trapping centers, as concluded from the exponential fit of photo-induced current decay, Fig. 2. Then, close to grain boundary, trapping by the Eu^{3+} ions shall be less effective, keeping the current higher than in the case where they are preferentially located at SnO_2 lattice sites, as the case of $GaAs/SnO_2$:2 at%Eu, annealed at 400 °C. Another possible explanation for the lower resistivity obtained for the lower temperature treated heterojunction comes from the SEM picture of sample surfaces as presented in Fig. 4. The presence of a higher amount of nucleated particles in the sample annealed at higher temperature may increase the electron scattering, which becomes more effective, contributing to the observed lower conductivity of this sample.

5. Summary and conclusion

Two $GaAs/SnO_2$:2%Eu heterojunctions, thermally annealed at 200 °C/1 h and 400 °C/20 min present distinct behavior related to electrical and emission properties. Conductivity for the sample annealed at 200 °C is much higher and the deepest level, ionized around room temperature is 79 meV, whereas for the sample annealed at 400 °C, this level is 98 meV below the conduction band bottom. These values could explain the difference in the current magnitude for these two samples. Surprisingly, the sample treated at lower temperature and, then, with smaller crystallites, presents a shallower energy level, which is more easily ionized, leading to a higher current. This feature may be related to a less effective trapping by the Eu^{3+} ions, located close to grain boundary, in the case of the lower temperature annealed heterostructure, or with a less effective electron scattering, due to presence of a smaller amount of large sized particles.

The decay of photo-induced current, at room temperature, when excited with light source with energies lower than 1.65 eV, for the heterojunction $GaAs/SnO_2$:2%Eu, thermally annealed at 200 °C/1 h, is 48.8% from the initial value, after 600 s. By comparison, the sample $GaAs/SnO_2$:2%Eu, thermally annealed at 400 °C/20 min the decay is 54.2% from the initial value. The larger variation (current decay) takes place for the sample annealed at 400 °C/20 min, which also presents higher activation energy (98 meV). This result is interesting because the deeper defect level acts as a more efficient driving force for retrapping the excited electrons. Although the light energy assures that only intrabandgap levels of SnO_2 top layer are excited, the intensity is high enough to penetrate the GaAs layer and generate electron-hole pairs in this material. There is also the possibility of excitation of the 2DEG at the interface. The data fitting seems to indicate that although the grain boundary scattering dominates the mobility, this term is time-independent, and the data fitting suggests the inclusion of time dependent terms, such as capture by more than one center, or ionized impurity scattering contribution.

Concerning the PL data, as the annealing temperature increases, the main Eu^{3+} transition change from $^5D_0 \rightarrow {}^7F_2$ (about 618 nm), related to ions located at asymmetric sites such as boundary layer, to $^5D_0 \rightarrow {}^7F_1$ (around 590 nm), related to ion located at symmetric sites, for example Eu^{3+} substitutional to Sn^{4+} in the SnO_2 lattice.

The luminescence from Eu-doped oxides, in the form of thin films provides accessibility to construction and operation of luminescent and electroluminescent devices, unlike samples in the form of powder. In the case of electroluminescence, the electrical transport characteristics shown in this paper are highly requested. The combination of SnO_2 with GaAs in the form of heterojunction films provides emission even for samples thermally annealed at lower temperatures, unlike samples of isolated SnO_2 films, which must be annealed at much higher temperatures. In this latter case, a much more expensive quartz substrate is needed, making the process of producing electroluminescent films unviable for technological application.

Acknowledgements

The authors would like to thank Prof. Margarida J. Saeki for very useful discussions, and Prof. Maximo Siu Li for PL measurements and fruitful discussions. They also thank the financial support of the Brazilian agencies: CAPES, CNPq and FAPESP.

References

[1] M. Ishii, S. Komuro, T. Morikawa, Study on atomic coordination around Er doped into anatase and rutile TiO_2:Er-O clustering dependent on the host crystal phase, J. Appl. Phys. 94 (2003) 3823–3827.
[2] E. Dien, J.M. Laurent, A. Smith, Comparison of optical and electrical characteristics of SnO_2-based thin films deposited by pyrosol from different tin precursors, J. Eur. Ceram. Soc. 19 (1999) 787–789.
[3] E.A. Morais, L.V.A. Scalvi, A. Tabata, J.B.B. Oliveira, S.J.L. Ribeiro, Photoluminescence of Eu^{3+} ion in SnO_2 obtained by sol–gel, J. Mater. Sci. 43 (2008) (345-249).
[4] K. Strauss, T.A. Destefani, F.A. Sigoli, I.O. Mazali, Crystalline SnO_2 nanoparticles size probed by Eu^{3+} luminescence, Cryst. Growth Des. 11 (2011) 4511–4516.
[5] E.A. Morais, L.V.A. Scalvi, S.J.L. Ribeiro, V. Geraldo, Poole-Frenkel effect in Er doped SnO_2 thin films deposited by sol-gel-dip-coating, Phys. Status Solidi A 202 (2005) 301–308.
[6] A. Kar, A. Patra, Optical and electrical properties of Eu^{3+}-doped SnO_2 nanocrystals, J. Phys. Chem. C 113 (2009) 4375–4380.
[7] G. Du, Y. Cui, X.C. Xia, X.P. Li, H.C. Zhu, B.L. Zhang, Y.T. Zhang, Y. Ma, Visual-infrared electroluminescence emission from ZnO/GaAs heterojunctions grown by metal-organic chemical vapor deposition, Appl. Phys. Lett. 90 (2007) 243504–243506.

[8] S.T. Tan, J.L. Zhao, S. Iwan, X.W. Sun, X. Tang, J. Ye, M. Bosman, L.J. Tang, G.Q. Lo, K.L. Teo, n-ZnO/n-GaAs heterostructured white light-emitting diode: nanoscale interface analysis and electroluminescence studies, IEEE Trans. Electron Devices 57 (2010) 129–133.
[9] E. Cuculescu, I. Evtodiev, M. Caraman, Non-equilibrium charge carriers generation - recombination mechanisms at the interface of the SnO_2/GaSe heterojunction, Thin Solid Films 517 (2009) 2515–2518.
[10] C.H. Lee, G.H. Lee, A.M. Zande, W. Chen, Y. Lu, M. Hand, X. Cui, G. Arefe, C. Nuckols, T.F. Heinz, J. Guo, J. Hone, P. Kim, Atomically thin p-n junctions with van der walls heterointerfaces, Nat. Nanotechnol. 9 (2014) 676–681.
[11] R. Cheng, D. Li, H. Zhou, C. Wang, A. Yin, S. Jiang, Y. Liu, Y. Chen, Y. Huang, X. Duan, Electroluminescence and photocurrent generation from atomically sharp WSe_2/MoS_2 heterojunction p-n diodes, Nano Lett. 14 (2014) 5590–5597.
[12] H. Li, H. Yu, X. Quan, S. Chen, H. Zhao, Improved photocatalytic performance of heterojunction by controlling the contact facet: High electron transfer capacity between TiO_2 and the{110} facet of $BiVO_4$ caused by suitable energy band alignment, Adv. Funct. Mater. 25 (2015) 3074–3080.
[13] Y.C. Zheng, S. Yang, X. Chen, Y. Chen, Y. Hou, H.G. Yang, Thermal-induced Volmer—Weber growth behavior for planar heterojunction perovskites solar cells, Chem. Mater. 27 (2015) 5116–5121.
[14] S. Yang, Y. Chen, Y.C. Zheng, X. Chen, Y. Hou, H.G. Yang, Formation of high-quality perovskite thin film for planar heterojunction solar cells, RSC Adv. 5 (2015) 69502–69508.
[15] H.Z. Yu, C.V. Thompson, Grain growth and complex stress evolution during Volmer–Weber growth of polycrystalline thin films, Acta Mater. 67 (2014) 189–198.
[16] K. Horn, Electronic structure of semiconductor surfaces, cap. 7, in: K. Horn, M. Scheffler (Eds.), Handbook of Surface Science, Vol 2, Elsevier 2000, p. 385.
[17] T.F. Pineiz, L.V.A. Scalvi, M.J. Saeki, E.A. Morais, Interface formation and electrical transport in SnO_2:Eu^{3+}/GaAs heterojunction deposited by sol–gel dip-coating and resistive evaporation, J. Electron. Mater. 39 (2010) 1170–1176.
[18] T.F. Pineiz, E.A. Morais, L.V.A. Scalvi, C.F. Bueno, Interface formation of nanostructured heterojunction SnO_2:Eu/GaAs and electronic transport properties, Appl. Surf. Sci. 267 (2013) 200–205.
[19] C.F. Bueno, L.V.A. Scalvi, M.S. Li, M.J. Saeki, Luminescence of Eu^{3+} in the thin film heterojunction GaAs/SnO_2, Opt. Mater. 5 (2015) 59–72.
[20] N.N. Iosad, G.J. Ruis, E.V. Morks, A.F. Morpurgo, N.M. van der Pers, P.F.A. Alkemad, V.G.M. Sivel, Dielectric response of sputtered transition metal oxides, J. Appl. Phys. 95 (2004) 8087–8091.
[21] T.W. Dobson, L.V.A. Scalvi, J.F. Wager, Transient decay of persistent photoconductivity in $Al_{0.3}Ga_{0.7}As$, J. Appl. Phys. 68 (1990) 601–605.
[22] E.A. Morais, L.V.A. Scalvi, V. Geraldo, R.M.F. Scalvi, S.J.L. Ribeiro, C.V. Santilli, S.H. Pulcinelli, Electro-optical properties of Er-doped SnO_2 thin films, J. Eur. Ceram. Soc. 24 (2004) 1857–1860.
[23] E.R. Viana, J.C. Gonzalez, G.M. Ribeiro, A.G. Oliveira, Photoluminescence and high-temperature persistent photoconductivity experiments in SnO_2 nanobelts, J. Phys. Chem. C 117 (2013) 7844–7849.
[24] S. Chitra, D. Easwaramoorthy, S.N. Jayanthi, S. Shanthi, Structural and optical properties of pure and transition metal ion doped SnO_2 quantum dots, Int. J. Chem. Tech. Res. 6 (2014) 4722–4728.
[25] E.A. Morais, L.V.A. Scalvi, Decay of photo-excited conductivity of Er-doped SnO_2 thin films, J. Mater. Sci. 42 (2007) 2216–2221.
[26] E.A. Floriano, L.V.A. Scalvi, J.R. Sambrano, A. Andrade, Decay of photo-induced conductivity in Sb-doped SnO_2 thin films, using monochromatic light of about bandgap energy, Appl. Surf. Sci. 267 (2013) 164–168.
[27] E.A. Morais, L.V.A. Scalvi, A.A. Cavalheiro, A. Tabata, J.B.B. Oliveira, Rare earth centers properties and electron trapping in SnO_2 thin films produced by sol–gel route, J. Non-Cryst. Solids 354 (2008) 4840–4845.
[28] V. Geraldo, V. Briois, L.V.A. Scalvi, C.V. Santilli, EXAFS investigation on Sb incorporation effects to electrical transport in SnO_2 thin films deposited by sol-gel, J. Eur. Ceram. Soc. 27 (2007) 4265–4268.
[29] D.H. Zhang, H.L. Ma, Scattering mechanisms of charge carriers in transparent conducting oxide films, Appl. Phys. A Mater. Sci. Process. 62 (1996) 487–492.
[30] C.F. Bueno, D.H.O. Machado, T.F. Pineiz, L.V.A. Scalvi, Photo-induced conductivity of heterojunction GaAs/rare-earth doped SnO_2, Mater. Res. 16 (2013) 831–838.
[31] D. Chattopadhyay, H.J. Queisser, Electron scattering by ionized impurities in semiconductors, Rev. Mod. Phys. 53 (1981) 745–768.
[32] N. Takimoto, On the screening of impurity potential by conduction electrons, J. Phys. Soc. Jpn. 14 (1959) 1142–1158.
[33] L.V.A. Scalvi, E. Minami, The energy barrier for electron trapping in $Al_xGa_{1-x}As$, Phys. Status Solidi A 139 (1993) 145–152.
[34] L. Yu, H. Song, S. Lu, Z. Liu, L. Yang, T. Wang, X. Kong, Thermal quenching characteristics in $LaPO_4$:Eu nanoparticles and nanowires, Mater. Res. Bull. 39 (2004) 2083–2088.
[35] G.E.S. Brito, S.J.L. Ribeiro, V. Briois, J. Dexpert–Ghys, C.V. Santilli, S.H. Pulcinelli, Short Range Order Evolution in the Preparation of SnO_2 Based Materials, J. Sol-Gel Sci. Technol. 8 (1997) 261–268.
[36] S.J.L. Ribeiro, S.H. Pulcinelli, C.V. Santilli, SnO_2:Eu nanocrystallites in SnO_2 monolithic xerogels, Chem. Phys. Lett. 190 (1992) 64–66.
[37] E.A. Morais, S.J.L. Ribeiro, L.V.A. Scalvi, C.V. Santilli, L.O. Ruggiero, S.H. Pulcinelli, Y. Messaddeq, Optical characteristics of Er–Yb doped SnO_2 xerogels, J. Alloys Compd. 344 (2002) 217–220.
[38] M. Yu, J. Lin, J. Fu, H.J. Zhang, Y.C. Han, Sol–gel synthesis and photoluminescent properties of $LaPO_4$:A (A-Eu^{3+}, Ce^{3+}, Tb^{3+}) nanocrystalline thin films, J. Mater. Chem. 13 (2003) 1413–1419.